A Method for the Rapid Generation of Nonsequential Light-Response Curves of Chlorophyll Fluorescence[1]

João Serôdio*, João Ezequiel, Jörg Frommlet, Martin Laviale, and Johann Lavaud

Departamento de Biologia and Centro de Estudos do Ambiente e do Mar, Universidade de Aveiro, Campus de Santiago, 3810–193 Aveiro, Portugal (J.S., J.E., J.F., M.L.); and UMR 7266 Littoral, Environnement et Sociétés, CNRS-University of La Rochelle, Institute for Coastal and Environmental Research, 17 000 La Rochelle, France (J.L.)

ORCID ID: 0000-0002-9047-1740 (J.S.).

Light-response curves (LCs) of chlorophyll fluorescence are widely used in plant physiology. Most commonly, LCs are generated sequentially, exposing the same sample to a sequence of distinct actinic light intensities. These measurements are not independent, as the response to each new light level is affected by the light exposure history experienced during previous steps of the LC, an issue particularly relevant in the case of the popular rapid light curves. In this work, we demonstrate the proof of concept of a new method for the rapid generation of LCs from nonsequential, temporally independent fluorescence measurements. The method is based on the combined use of sample illumination with digitally controlled, spatially separated beams of actinic light and a fluorescence imaging system. It allows the generation of a whole LC, including a large number of actinic light steps and adequate replication, within the time required for a single measurement (and therefore named "single-pulse light curve"). This method is illustrated for the generation of LCs of photosystem II quantum yield, relative electron transport rate, and nonphotochemical quenching on intact plant leaves exhibiting distinct light responses. This approach makes it also possible to easily characterize the integrated dynamic light response of a sample by combining the measurement of LCs (actinic light intensity is varied while measuring time is fixed) with induction/relaxation kinetics (actinic light intensity is fixed and the response is followed over time), describing both how the response to light varies with time and how the response kinetics varies with light intensity.

Light-response curves (LCs) are widely used in plant physiology for the quantitative description of the light dependence of photosynthetic processes (Henley, 1993). Originally developed for characterizing the response of steady-state photosynthesis to ambient irradiance (Smith, 1936), LCs attained widespread use following the introduction of pulse amplitude-modulated (PAM) fluorometry (Schreiber et al., 1986). Through its ability to monitor the activity of PSII, this technique allows the generation of LCs of relative electron transport rate (rETR; Schreiber et al., 1994), a noninvasive and real-time indicator of photosynthetic activity, shown to be a close proxy for biomass-specific rates of photosynthesis (Genty et al., 1989; Seaton and Walker, 1990). Due to the considerable operational advantages of PAM fluorometry, LCs of rETR became the most common means to quantitatively characterize the light response of photosynthetic activity in plants as well as in virtually all types of photoautotrophic organisms (Rascher et al., 2000; Serôdio et al., 2005; Ye et al., 2013).

Ideally, LCs should be based on independent measurements of the parameter under study. For example, in ^{14}C-based methods of measuring photosynthetic rates in phytoplankton, this is the case (Johnson and Sheldon, 2007). It is also possible to generate LCs from PAM measurements in independent replicated samples (Lavaud et al., 2007), but the need to cover a wide range of actinic light levels with appropriate replication makes this approach very time and sample consuming. Therefore, in most cases, LCs are generated sequentially, by exposing the same sample to a (usually increasing) range of irradiance levels (Schreiber et al., 1994).

An often overlooked consequence of sequential LCs is that the response of the sample under each light level is strongly affected by its exposure to previous light levels (Perkins et al., 2006; Herlory et al., 2007; Ihnken et al., 2010). Therefore, LCs constructed in this way are dependent not only on the absolute light levels applied during the generation of the curve but also on the duration of the exposure to each light level and on their order of application. The effects of non-independence between measurements are expected to

[1] This work was supported by the Fundação para a Ciência e a Tecnologia (grant no. SFRH/BSAB/962/2009 to J.S., grant no. SFRH/BD/44860/2008 to J.E., and projects MigROS [grant no. PTDC/MAR/112473/2009 to M.L.] and SeReZoox [grant no. PTDC/MAR/113962/2009 to J.F.]), by the Centre National de la Recherche Scientifique (Chercheurs Invités program grants to J.S. and J.L.), by the French consortium Contrat Plan Etat-Région-Littoral, and by the Egide/Campus France Partenariat Hubert-Curien Pessoa exchange program (grant no. 27377TB to J.S. and J.L.).

* Address correspondence to jserodio@ua.pt.

The author responsible for distribution of materials integral to the findings presented in this article in accordance with the policy described in the Instructions for Authors (www.plantphysiol.org) is: João Serôdio (jserodio@ua.pt).

www.plantphysiol.org/cgi/doi/10.1104/pp.113.225243

be intensified in the case of rapid light curves (Schreiber et al., 1997; White and Critchley, 1999), curves generated by reducing the duration of each light step, normally to just 10 to 30 s (Rascher et al., 2000; Ralph and Gademann, 2005; Perkins et al., 2006). The short duration of the light steps do not allow the sample to reach a steady state under each light level, thus being largely influenced by previous light history (Serôdio et al., 2006; Ihnken et al., 2010; Lefebvre et al., 2011).

Here, we present an alternative method to generate LCs of fluorescence parameters from truly independent, nonsequential measurements. The method is based on the spatial separation of the different levels of actinic light used to construct the light curve and uses the capabilities of chlorophyll fluorescence imaging systems to simultaneously measure the fluorescence emitted by samples exposed to different irradiance levels. This approach enables light curves to be measured very rapidly, as it only requires that the samples are exposed to the different actinic light levels for the desired period of time (e.g. to reach a steady-state condition) before a single saturating pulse is applied to measure the fluorescence response of all samples simultaneously. By reducing significantly the time required for the generation of LCs, this approach makes it possible to easily characterize the dynamic light response by simultaneously tracing the fluorescence response under different light intensities over time.

This work demonstrates the proof of concept for the generation of LCs through the combined use of (1) sample illumination with spatially separated light beams of different intensity, through the use of a digital projector as a source of actinic light, and (2) imaging chlorophyll fluorometry. The application of the method is illustrated for intact plant leaves, but its general principle of operation is applicable to any other type of photosynthetic samples, such as macroalgae, lichen, or suspensions of microalgae or chloroplasts.

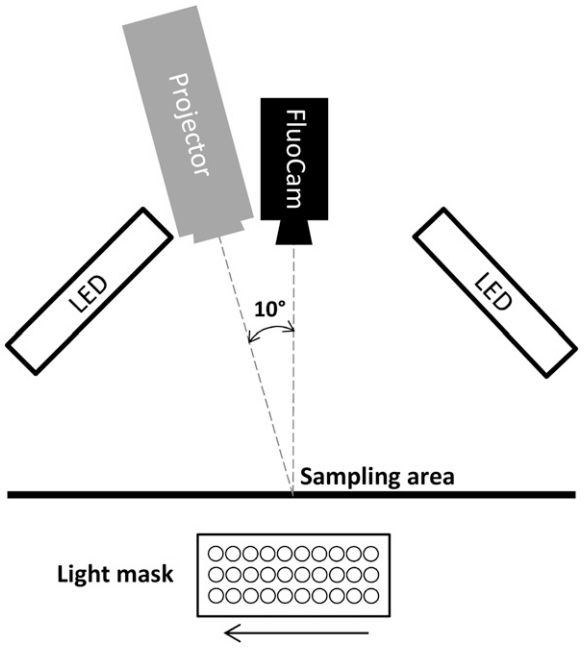

Figure 1. Scheme showing the relative positions of the digital projector, the imaging chlorophyll fluorometer components (the CCD camera and the LED panels emitting saturating pulses), the sampling area, and the projected actinic light mask (not at scale). For simplicity, two additional LED panels emitting nonactinic, measuring light, positioned perpendicular to the panels shown, were omitted. The horizontal arrow indicates increasing levels of actinic light in the light mask.

RESULTS

Rationale of the Method

The method is based on the illumination of replicated samples with actinic light of different intensities and on the simultaneous detection of the induced fluorescence by an imaging chlorophyll fluorometer. The method requires a number of conditions to be met.

A fundamental requirement is that the illumination of the samples with different levels of actinic light must not interfere with its exposure to the measuring light and saturation pulses. For this reason, the best solution is to project on the samples the required combination of actinic light levels ("light mask"; see below) using a light source positioned from such a distance that the measuring light and saturating pulses can reach the samples unimpeded. This approach also allows for the measuring light and the saturating pulses to illuminate the sample while it is exposed to the actinic light, a critical condition of the saturating pulse method (Schreiber et al., 1986). Nonetheless, in order to be useful for the generation of a light curve, the fluorescence response must be related solely to the different actinic light levels applied. This implies the use of either replicated samples (e.g. microalgae culture on a multiwell plate) or a homogenous single sample (e.g. whole leaf). In the latter case, however, the independence of the measurements may be compromised by light scattering within the sample (leaf tissue), causing light spillover between adjacent areas illuminated with different actinic light levels (see below).

In this study, a digital projector was used as a source of actinic light (Fig. 1; see below for details), due to the large potential advantages deriving from the versatility provided by the digital control of light output. However, the novelty of this approach in plant photophysiology required extensive testing regarding both the emitted light and the detection of the fluorescence response.

Regarding light output, the digital projector used in this study was analyzed concerning the spectral characteristics of the emitted light. An important condition for any light source to be used for generating LCs is that the light spectrum does not change significantly over the range of light intensities applied. Otherwise,

substantial distortions in the light curve shape may be induced, as the photosynthetic light absorption varies significantly along the different regions of the spectrum. This was tested by measuring the spectrum of light emitted at the various output intensities used for generating light curves.

The use of a digital projector was also tested regarding the potential interference on the detection of the fluorescence signals. Images produced by digital projectors are known to suffer from flickering, which, although imperceptible to the human eye, may affect the determination of steady-state fluorescence (F_s) and maximum PSII fluorescence in the light-adapted state (F_m') and the calculation of fluorescence indices like PSII effective quantum yield ($\Delta F/F_m'$) or nonphotochemical quenching (NPQ). Preliminary tests were made on the two main types of digital projector, Liquid-Crystal Display (LCD) and Digital Light Processing (DLP) projectors. In LCD projectors, images are generated from light beams (three, each of one primary color) passing through separate LCD panels made of a large number of liquid crystals, each corresponding to a pixel in the projected image. The three beams are later combined into a single, full-color beam. In the case of DLP technology, the projected light beam arises from light reflected from a reflective surface made of a large number of small mirrors (DLP chip), each corresponding to a pixel in the final image. The orientation of each mirror is controlled individually, determining the intensity of each pixel.

The interference of actinic light flickering on fluorescence measurements was tested by analyzing the fluorescence kinetics immediately before (determination of F_s level) and during (determination of F_m' level) the application of a saturating pulse on samples exposed to different actinic light intensities provided by the projector. DLP projectors exhibited a much higher intensity of flickering, making them impossible to use in this context. The study was thus carried out using a LCD projector (see below).

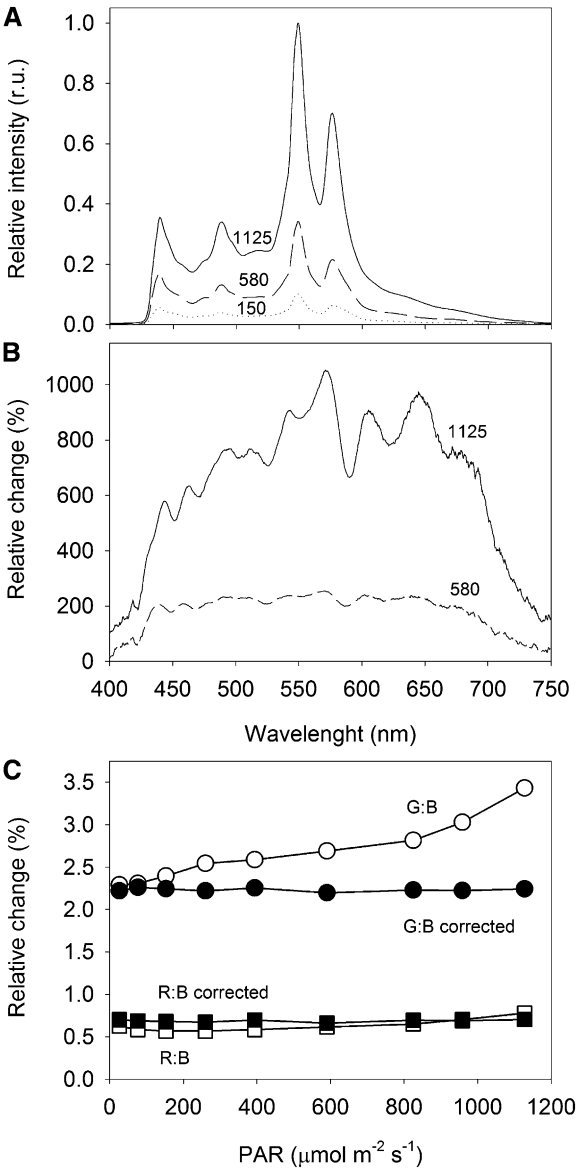

Figure 2. Variation of the light spectrum with intensity. A, Spectrum of the light emitted by the digital projector at different output intensities. Numbers represent PAR measured at the sample level (μmol m^{-2} s^{-1}). r.u., Relative units. B, Variation (%) of the light spectrum relative to the light projecting 150 μmol m^{-2} s^{-1} at the sample level. C, Comparison between the proportion of green:blue light (G:B) and red:blue light (R:B) for the different PAR levels used for generating LCs, before and after spectral correction through manipulation of the RGB code.

Actinic Light Spectrum

The spectrum of the light emitted by the digital projector covered the wavelength range of photosynthetically active radiation (PAR), from approximately 430 to over 700 nm (Fig. 2A). The projected light was rich in photosynthetically active blue light, its spectrum showing a distinct peak at 440 nm, but poorer in red light (650- to 700-nm band). The spectrum showed two large peaks in the green-yellow region, centered at 550 and 580 nm. Very little thermal radiation (above 750 nm) was emitted, even when applying the highest PAR levels. This means that the projector used was a suitable source of cold actinic light, which did not induce differences in temperature over the different areas of actinic light (AALs).

The light spectrum was found to change substantially when varying the lamp output intensity (Fig. 2B). Below moderate PAR values (e.g. 580 μmol m^{-2} s^{-1} at the sample level), irradiance increased equally over most of the spectral range (flat spectrum from 440 to 675 nm, when compared with 150 μmol m^{-2} s^{-1}). But for higher lamp outputs (e.g. 1,125 μmol m^{-2} s^{-1}), the spectrum was increasingly enriched in green-yellow light (mainly green, 525–590 nm, and yellow-orange, 600–660 nm), becoming comparatively poorer in photosynthetically active blue and red light. The variation of the light spectrum with intensity may represent a

major problem for the generation of LCs. Because the yellow-green light that dominates the spectrum when applying higher light levels is poorly absorbed by photosynthetic pigments, the corresponding values of $\Delta F/F_m'$ (or rETR) will appear overestimated when plotted against the measured PAR levels. As a result, rETR LCs may show an inflection in the light-saturated region, showing an increase of rETR values when stabilization or even a decrease would be expected.

This problem was addressed by manipulating the spectrum of emitted light so that the proportions of red, green, and blue light (RGB) regions of the spectrum remained approximately constant over the whole range of light intensities applied. This was achieved through an iterative process of changing the Microsoft Visual Basic code controlling the RGB ratio of the images produced by the projector, measuring the emitted spectrum, and calculating the resulting proportions of RGB spectral regions. The RGB code allowed us to independently control the spectral ranges of 400 to 486 nm (blue), 487 to 589 nm (green-yellow), and 590 to 690 nm (red). This procedure was repeated until the same proportions of RGB were obtained in the emitted light for the various PAR levels that were used for generating LCs. An average proportion for red:green:blue of 0.7:2.2:1 was used (Fig. 2C), which, by having a higher proportion of yellow-green light, ensured the emission of high maximum PAR levels (1,125 μmol m^{-2} s^{-1} at the sample level).

Actinic Light Flickering

The projector light showed noticeable flickering, causing obvious fluctuations in the fluorescence trace (Fig. 3). Light flickering caused interferences at 1.8-s intervals, more pronounced under higher actinic light levels, when it significantly affected the correct determination of both F_s and F_m' levels. Using the data of Figure 3 as an example, if the full fluorescence record was considered for calculating F_s and F_m', it would result in an underestimation of $\Delta F/F_m'$ values of 3.0% and 22.3%, for 260 and 850 μmol m^{-2} s^{-1}, respectively. To avoid these confounding effects, it was necessary to analyze the fluorescence recording for each individual measurement (immediately before and during a saturating pulse) and exclude the affected data points.

Application to Intact Leaves

The method was tested on intact leaves of plants acclimated to different light regimes, expected to show contrasting features in LCs of fluorescence. Figure 4 shows chlorophyll fluorescence images resulting from the application of an actinic light mask to leaves of high light (HL)-acclimated common ivy (*Hedera helix*; Fig. 4, A–C) and low light (LL)-acclimated weeping fig (*Ficus benjamina*; Fig. 4, D–F) for a known period of time.

Images of F_s and F_m' of ivy (Fig. 4, A and B) showed some degree of heterogeneity, with higher absolute pixel values in the central region of the leaf and lower values

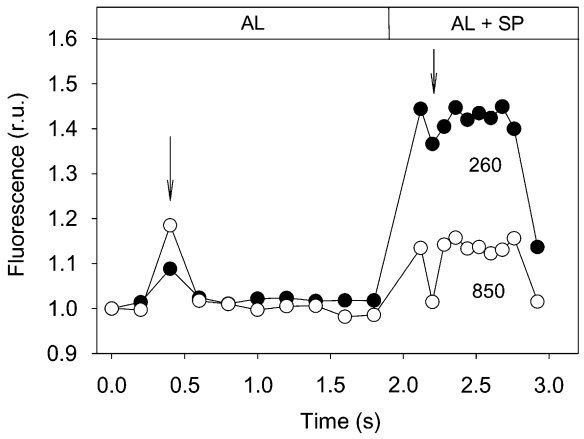

Figure 3. Effects of digital projector light flickering (arrows) on the recording of chlorophyll fluorescence immediately prior to (for the determination of F_s) and during (for the determination of F_m') a saturating pulse (SP) emitted by a sample exposed to actinic light (AL) of 260 and 850 μmol m^{-2} s^{-1}. Values were normalized to the first measurement. r.u., Relative units.

in the extremities. This was due to the large leaf size in relation to the projected light fields of measuring light and saturating pulses. However, this did not affect significantly the determination of the ratio $\Delta F/F_m'$, which remained relatively constant throughout the whole leaf (varying between 0.79 and 0.83; Fig. 4C). In the case of weeping fig, although the smaller leaf size helped reduce the effects of light field heterogeneity, spatial variability was still noticeable due to certain leaf anatomical features (e.g. central vein). Again, while this was evident for F_s and F_m' images, the effect mostly disappeared when the ratio $\Delta F/F_m'$ was calculated (Fig. 4F).

The application of the actinic light mask on intact leaves resulted in well-defined areas of induced fluorescence response. Particularly for higher light levels, each AAL showed a noticeable outer ring of pixels of intensity intermediate between background values (not illuminated areas) and fully illuminated areas (center of each AAL). The resulting fluorescence images showed a clearly different pattern of response to actinic light in the two plants. While for the HL-acclimated ivy, little effects were observed on F_s, which remained virtually constant over the range of PAR levels applied (Fig. 4A), for the LL-acclimated weeping fig, a large variation in F_s was observed (Fig. 4D). Also regarding F_m', it was clear that in ivy the exposure to high light caused a larger decrease than in weeping fig. As a consequence, clear differences were also observed regarding $\Delta F/F_m'$ values, which reached lower values in the LL-acclimated plant. It may be noted that there was a high similarity between replicated AAL and that, as in the case of weeping fig, heterogeneities in F_s and F_m' had little effect on $\Delta F/F_m'$ (Fig. 4, D–F).

These fluorescence images are also useful to illustrate the variability regarding light scattering within the leaf and its impact on the applicability of the method to

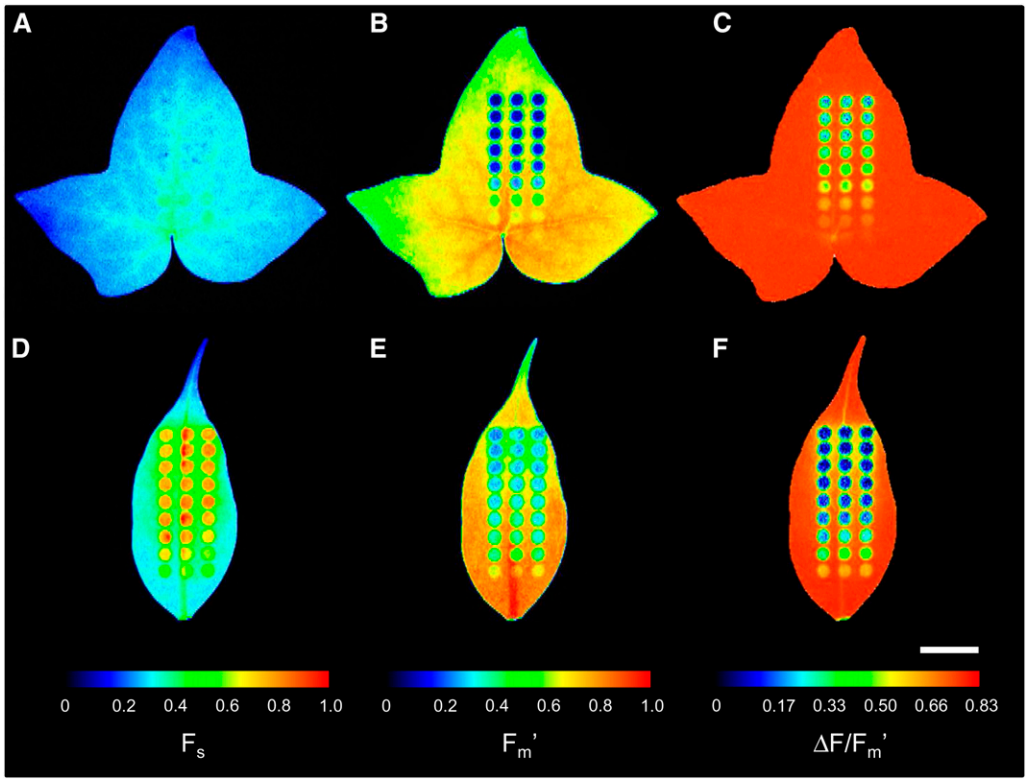

Figure 4. Example of the application of an actinic light mask on leaves of HL-acclimated ivy (A–C) and LL-acclimated weeping fig (D–F). Images (false color scale) show F_s (A and D), F_m' (B and E), and $\Delta F/F_m'$ (C and F) measured after 6 min of exposure to the light mask following a period of 20 min in the dark. Fluorescence levels F_s and F_m' were normalized to the range of pixel values in each leaf. Bar = 1 cm.

intact leaves. Ivy leaves showed very low spillover between adjacent AALs, as deduced from the similarity between the pixel values of the areas between AALs and of the background (parts of the leaf distant from AALs; Fig. 4, B and C). Notably, larger spillover effects were observed on the lower (abaxial) surface of the ivy leaves (data not shown). In contrast with ivy, leaves of weeping fig showed a much larger light spillover around AALs. Both for F_s and F_m', the areas around AALs showed pixel values clearly different from the background values (Fig. 4, D and E). However, this did not seem to affect significantly the determination of F_s, F_m', or $\Delta F/F_m'$ in each area of interest (AOI), as no asymmetry was evident in pixel intensity within the AOI of the mask's outer arrays.

LCs: "Single-Pulse Light Curves"

After defining AOIs matching the projected AALs (Fig. 4), the values of F_s and F_m' were determined for the various actinic light levels. These values were used to calculate the indices $\Delta F/F_m'$, rETR, and NPQ, which, when plotted against incident actinic light, resulted in LCs (Fig. 5). These single-pulse light curves (SPLCs), despite requiring just a few minutes of light mask exposure and a single saturating pulse, nevertheless allowed us to characterize in detail the light response of the tested samples. Strong indications of the quality of these light curves were the low variability between replicates (measurements on AALs of identical PAR level, corresponding to the same row of the light mask) and the very good fit obtained with well-established mathematical models for describing rETR and NPQ versus irradiance level (E) curves.

The light-response patterns were consistent with the ones expected for LL and HL acclimation states. Departing from similar values for maximum photochemical efficiency of PSII in the dark-adapted state (F_v/F_m), $\Delta F/F_m'$ decreased more steeply with increasing irradiance in LL-acclimated weeping fig than in HL-acclimated ivy (Fig. 5, B and E). This resulted in distinct rETR versus E curves, with ivy showing higher values for initial slope (α) and, mainly, maximum rETR (approximately 5 times higher than for weeping fig). Also typical of the difference between LL- and HL-acclimated samples, the photoacclimation index (E_k) was much higher (more than double) in ivy than in weeping fig, in accordance with the fact that the former showed little sign of saturation even at 1,125 μmol m^{-2} s^{-1}, while the latter saturated at comparatively lower PAR values (Fig. 5E). Also in the case of

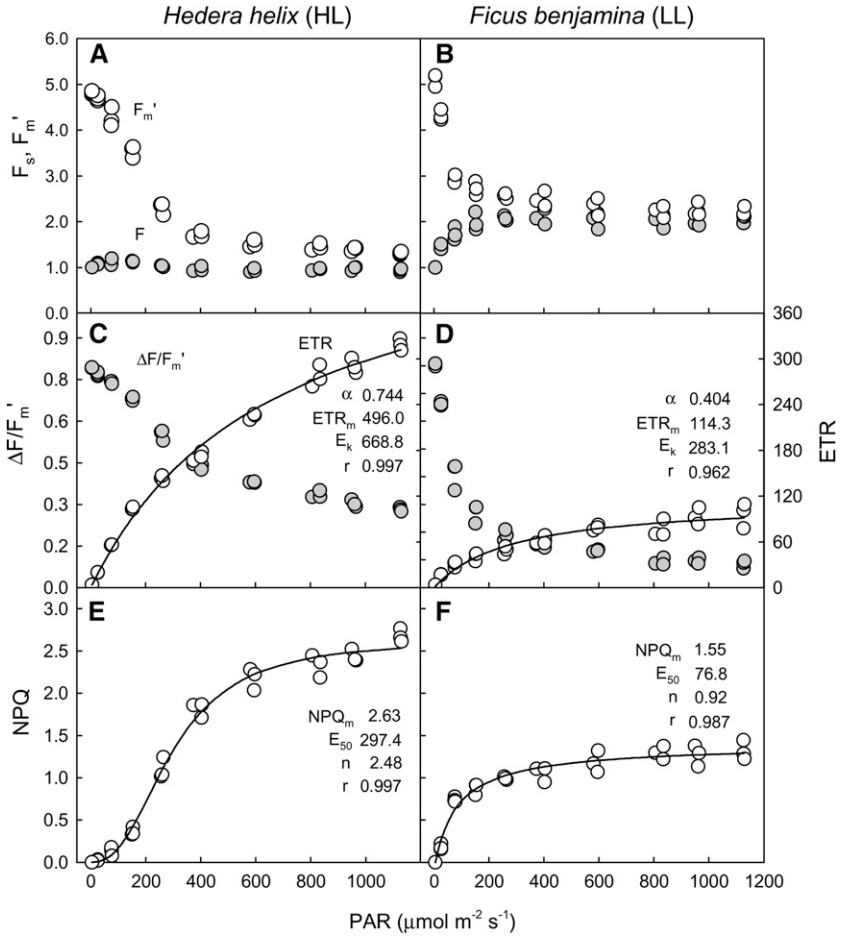

Figure 5. SPLCs. Fluorescence LCs were generated by the exposure of intact leaves of HL-acclimated ivy (A–C) and LL-acclimated weeping fig (D–F) to an actinic light mask (data of Fig. 4). LCs (data points) of fluorescence levels F_s and F_m' (A and D), $\Delta F/F_m'$ and rETR (B and E), and NPQ (C and F), fitted models (lines), and estimates of model parameters (Eqs. 1 and 2 for rETR and NPQ, respectively) are shown.

NPQ versus *E* curves, the results were in agreement with expected LL and HL acclimation patterns, with ivy reaching higher maximum NPQ values, requiring higher light levels for full development and higher sigmoidicity.

Dynamic Light Response

A further application of the method concerns the study of the temporal variation of the light response. Figure 6 shows an example of the variation over time of $\Delta F/F_m'$, rETR, and NPQ for ivy and weeping fig during light induction under different PAR levels. Confirming the very different light-response patterns observed before, this approach made it possible to additionally compare the temporal variation of the response of each fluorescence index. For the HL-acclimated ivy, $\Delta F/F_m'$ and rETR stabilized quite rapidly, reaching a steady state within 4 to 6 min upon light exposure (Fig. 6, A and C). The patterns of variation were essentially the same for the different light levels, although stabilization was faster for the samples exposed to lower PAR. For NPQ, steady state was reached only after 8 to 10 min, the induction pattern varying with the light level applied (Fig. 6E). In the case of LL-acclimated weeping fig, all indices took a longer time to reach a steady state (Fig. 6, B, D, and F). This was especially true for NPQ, which still increased for most of the PAR levels after 14 min of light exposure.

This approach is also particularly useful to follow the changes in the LC and to determine the time necessary for reaching of a steady state. This can be achieved by following the variation over time of the model parameters used to describe the LCs. Using the data set partially shown in Figure 6, Figure 7 shows the variation during light induction of the parameters of rETR and NPQ versus *E* curves. Regarding the rETR versus *E* curves, α was the parameter that showed a smaller variation over time, increasing modestly until reaching stable values after 6 and 10 min for ivy and weeping fig, respectively (Fig. 7A). In contrast, maximum rETR and E_k showed much larger fluctuations, particularly for ivy, requiring more than 8 to 10 min for reaching relatively stable values (Fig. 7, B and C). For the parameters of NPQ versus *E* curves, similar time periods of 6 to 10 min were necessary for reaching steady-state conditions (Fig. 7, D–F). However, despite the different induction patterns observed for HL- and LL-acclimated samples, most of the differences

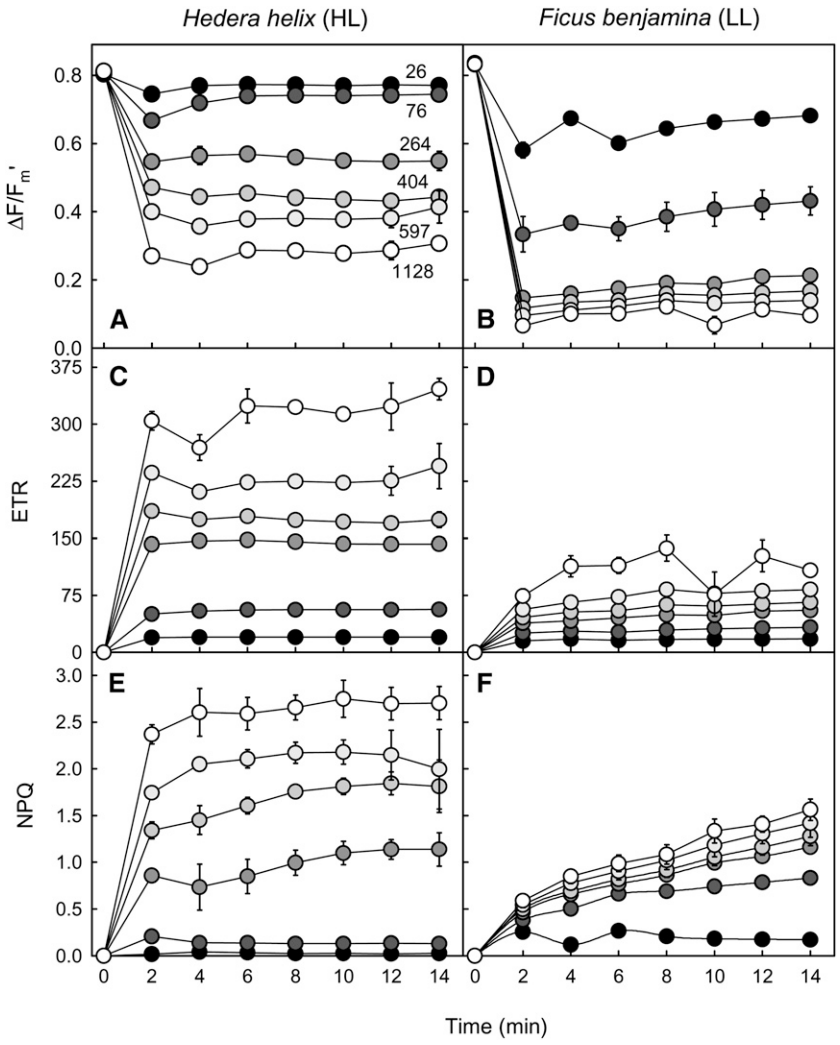

Figure 6. Dynamic light response. Variation over time is shown for the light response of fluorescence indices $\Delta F/F_m'$ (A and B), rETR (C and D), and NPQ (E and F). Measurements were made under selected PAR levels (numbers) as projected by using an actinic light mask on intact leaves of HL-acclimated ivy (A, C, and E) and LL-acclimated weeping fig (B, D, and F) leaves. Light exposure followed a 20-min dark exposure. Values shown are means of three replicated measurements. Error bars represent SE ($n = 3$).

observed at steady state were already present at the first measurements (2–4 min). This indicates that even a short 2- to 4-min period of light mask exposure may be sufficient to characterize LCs and detect differences between different light acclimation states.

Light Stress-Recovery Experiments and NPQ Components

This approach can be easily extended to carry out light stress-recovery experiments, in which samples are sequentially exposed to high light and then to darkness or low light, and the fluorescence kinetics during light induction and dark relaxation is used to evaluate the operation of photoprotective and photoinhibitory processes (Walters and Horton, 1991; Müller et al., 2001). Usually, only one light level is used, of arbitrarily chosen intensity (Rohácek, 2010; Serôdio et al., 2012). By applying a light mask conveying a range of actinic light, it becomes possible to study the fluorescence kinetics during light induction and dark relaxation for different PAR intensities simultaneously.

This is exemplified with the response of NPQ of LL-acclimated weeping fig during light induction and subsequent dark relaxation (Fig. 8). A large and detailed data set was obtained from a single leaf on the NPQ induction under various PAR levels (Fig. 8, A and B) and on its relaxation in the dark (Fig. 8, C and D). Figure 8 also highlights the two types of information that can be extracted from the same data set: LCs (Fig. 8, A and C) and induction/relaxation kinetics (Fig. 8, B and D). By applying the rationale used for the calculation of NPQ components, such a data set can be used to generate LCs of coefficients quantifying photoprotection capacity and susceptibility to photoinhibition (Guadagno et al., 2010). Figure 9 illustrates this approach by comparing the repartition of absorbed light energy in HL-acclimated ivy and LL-acclimated weeping fig. The former plant was shown to be able to use a larger fraction of absorbed light for photochemistry ($\Delta F/F_m'$; approximately 0.5 above 800 μmol m^{-2} s^{-1}; Fig. 9A), while nonphotoprotective NPQ components, Φ_{qT+qI}, the quantum yield of state transition and photoinhibitory quenching, remained under relatively low values (less

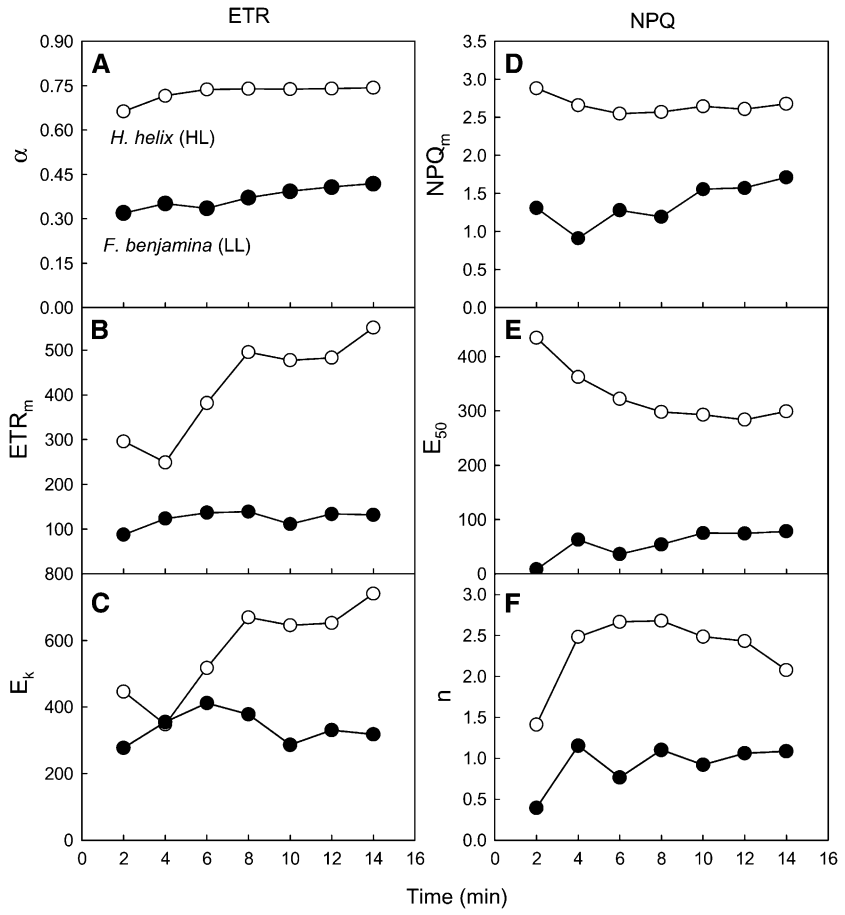

Figure 7. Dynamic light response: light induction of LCs. Variation over time is shown for the parameters of the LC of rETR (A–C; parameters of Eq. 1) and NPQ (D–F; parameters of Eq. 2) measured on intact leaves of HL-acclimated ivy and LL-acclimated weeping fig upon light exposure following a 20-min dark adaptation.

than 20%) and only started above 400 μmol m^{-2} s^{-1} (Fig. 9A). In contrast, for the LL-acclimated weeping fig, $\Delta F/F_m'$ was much lower throughout the light intensity range (less than 0.2 for PAR as low as 400 μmol m^{-2} s^{-1}; Fig. 9B), and NPQ started to increase under much lower PAR levels, reaching maximum values at approximately 200 μmol m^{-2} s^{-1} (Φ_{qT+qI} and Φ_C, the quantum yield of chlorophyll photophysical decay).

DISCUSSION

Method Assumptions

The purpose of this study was to demonstrate the proof of principle of the method, starting by identifying and testing the conditions required for its general application. The successful generation of nonsequential LCs using the combination of spatially separated actinic light beams and imaging chlorophyll fluorescence implied the verification of two types of assumptions: (1) assumptions associated with the projection of an actinic light mask and the detection of the induced fluorescence response, and (2) assumptions related to the use of a digital projector as a source of actinic light for this purpose. These conditions were tested and shown to be verified.

Regarding the projection of the actinic light mask, a very basic assumption of the method was that the samples exposed to different actinic light levels must have essentially the same inherent physiological light response, so that the fluorescence measured in different AALs may be attributed to the different PAR irradiances applied. In a way, this approach is opposed to the traditional use of chlorophyll fluorescence imaging systems: instead of applying a homogenous actinic light field to study heterogenous samples, here a heterogenous actinic light field is applied to study supposedly homogenous samples. The verification of this condition is mostly dependent of the physiological heterogeneity on the samples. In some cases, as for suspensions of microalgae or chloroplasts, samples can be prepared so that a uniform response can be ensured. However, in the case of leaves, it must be previously confirmed that the area to be used for the measurements is homogenous regarding its photophysiological responses. The results presented here show that the method can be successfully applied to whole leaves, through careful selection of uniform areas, in order to minimize the potentially confounding effects of within-leaf spatial inhomogeneity.

Another key assumption of the method is the independence of the measurements. This condition can be easily ensured by using optically separated samples,

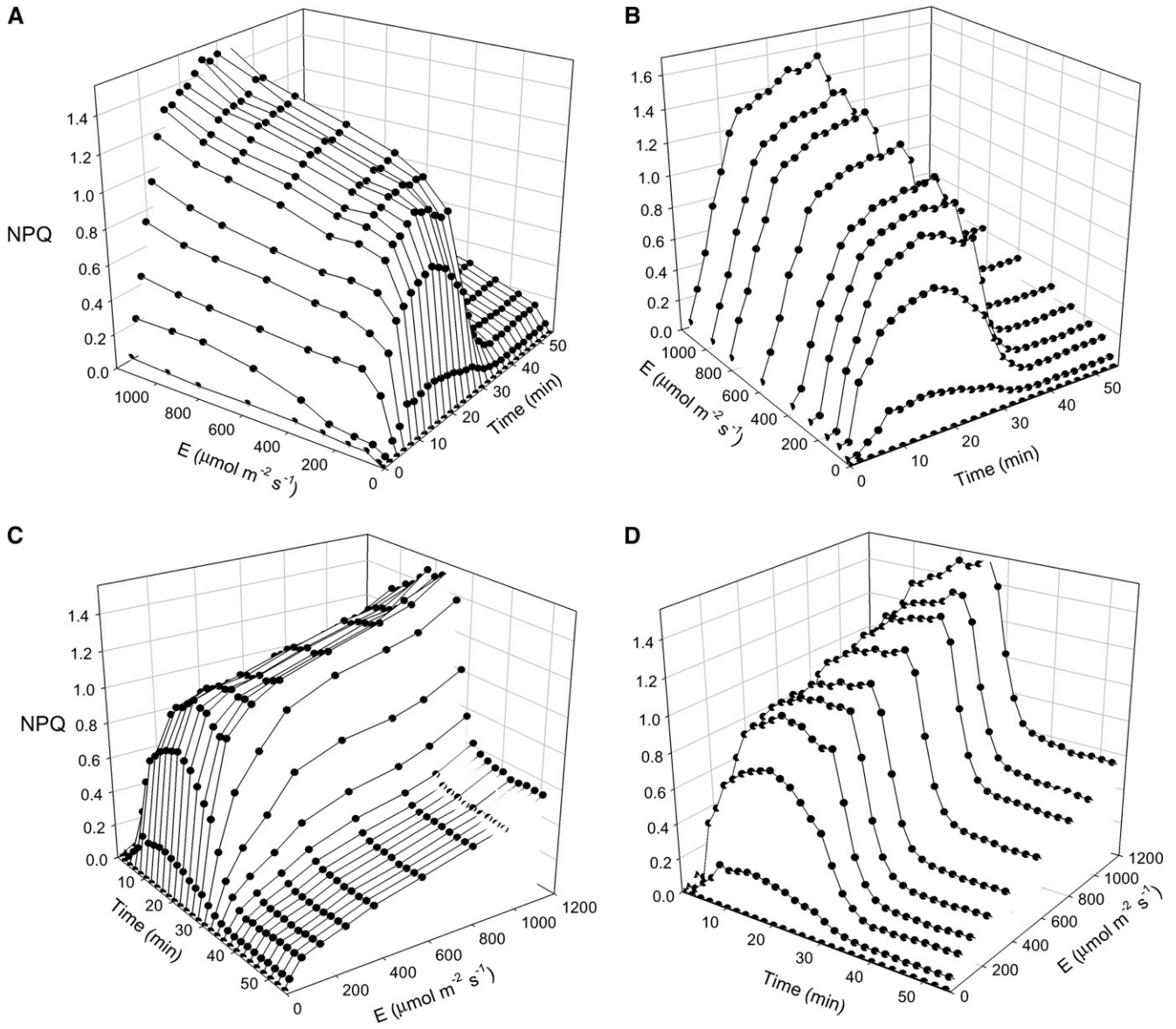

Figure 8. Dynamic light response: light stress-recovery experiment. The three-dimensional representation shows the time and light responses of NPQ of a LL-acclimated weeping fig leaf, highlighting the variation over time of the LC (A and C) or the light induction and dark relaxation kinetics (B and D). Light exposure followed a 20-min dark adaptation.

cell or chloroplast suspensions, or leaf discs on opaque multiwell plates impeding the transmission of light between adjacent samples. Potential problems are thus restricted to optically continuous samples such as whole leaves, where light spillover from one AAL to another may result in a lack of independence between adjacent AALs. This effect is analog to the time dependency between consecutive measurements during a sequential light curve. The results of the tests performed on leaves showed that this effect varied with species and with the leaf optical properties affecting the amount of internal light scattering. However, they also showed that light spillover can be greatly minimized through adequate design of the actinic light mask (see below).

Regarding the use of digital projectors as actinic light sources, two conditions appeared to be of most importance: the maintenance of a constant spectrum throughout the range of applied irradiances, and the elimination of effects of light flickering on fluorescence measurements. The maintenance of a constant spectrum is important because changes of the light spectrum can have substantial effects on $\Delta F/F_m'$, due to the variation of photosynthetic pigment absorptivity over different wavelength ranges. This effect may be observed when comparing rETR LCs induced by monochromatic light of different colors (Schreiber et al., 2012). In our case here, the enrichment of the green-yellow part of the spectrum is expected to cause an

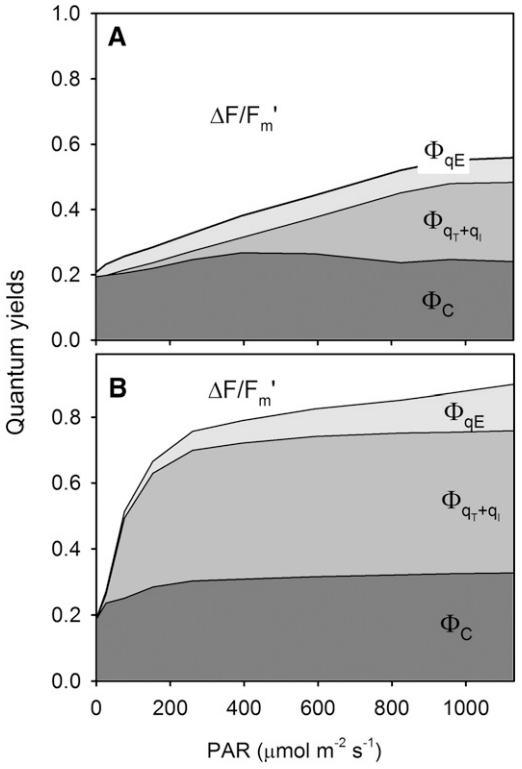

Figure 9. Dynamic light response. Light response of the quantum yield of PSII ($\Delta F/F_m'$) and NPQ components Φ_C (quantum yield of chlorophyll photophysical decay), Φ_{qE} (quantum yield of energy-dependent quenching) and Φ_{qT+qI} (quantum yield of state transition and photoinhibitory quenching) as calculated from the data of a light stress-recovery experiment carried on intact leaves of HL-acclimated ivy (A) and LL-acclimated weeping fig (B).

overestimation of $\Delta F/F_m'$ for the measured PAR, because light of these wavelengths is comparatively less absorbed by the dominating pigments such as chlorophyll *a* and *b*, thus inducing a smaller quenching of F_s and F_m'. Therefore, if the light spectrum varies between different AALs, this will likely result in a deformation of the shape of the LC, resulting in an artifactual absence of saturation or a decline under high light. As shown here, this problem may be tackled by digitally manipulating the spectrum of the emitted light. Despite some limitations, as only the spectral ranges corresponding to the RGB coding can be manipulated, this approach was shown to be sufficient to solve the effects of the changes in lamp output spectrum. Nevertheless, the need for this corrective procedure will depend on the magnitude of the induced effects, in turn dependent on the particular experimental and equipment conditions, such as projector and lamp type, and PAR levels to be used.

The elimination of the effects of light flickering is important because light flickering was shown to cause substantial interference in the fluorescence record, particularly for high actinic light levels, under which the difference between F_s and F_m' is smaller and the error associated with the determination of $\Delta F/F_m'$ is higher. While affected fluorescence values may be easily identified and eliminated from the calculation of F_s and F_m', this requires the possibility of accessing the raw fluorescence data, which may not be feasible with some PAM fluorometer models or software.

Light Mask Design

A crucial piece of the proposed experimental approach is the actinic light mask used to project spatially separated areas of actinic light. The light mask used in this study resulted from a large number of preliminary tests on several aspects, such as mask shape and dimension, as well as number, size, and disposition of the AALs. Its development followed some principles of general applicability in designing light masks for similar studies.

(1) Mask dimension. The shape and size of the light mask should consider the sample dimensions as well as the homogeneity of the measuring light and saturating pulse light fields. Smaller masks likely fit better within the zone of a homogenous light field sampling area, while they may also help to avoid heterogenous parts of the sample (e.g. major leaf veins). On the other hand, too small masks may limit both the total number and size of AALs and, by implying short distances between adjacent AALs, may increase light spillover and compromise the independency of the measurements.

(2) Number of AALs. A large number of AALs allows for a large number of light levels, which is useful for a good characterization of the light response and for replication, reducing variability and increasing the precision of parameter estimation. However, the number of AALs possible to accommodate will be limited by the total mask size and by the spillover between adjacent AALs. In this study, it was possible to accommodate 30 AALs, which resulted in a satisfactory number of data points along the light curve and a good level of replication. By effectively impeding light spillover (e.g. using opaque multiwell plates), this number could be significantly increased without increasing the light mask size.

(3) AAL distribution pattern. In principle, AALs should be randomly distributed throughout the light mask. This would minimize any systematic effects due to the AAL position within the possibly inhomogenous measuring light and saturating pulse fields. However, when spillover effects cannot be completely avoided, as in the case of whole leaves, better results were found by arranging the AAL along a gradient of light intensity, because in a randomized layout there is a high chance of having adjacent AALs of very different light intensities, resulting in substantial spillover and loss of measurement independence. When AALs are distributed along a light intensity gradient, the light intensity of adjacent AALs will be more similar, thus reducing the relative impact on each other. Besides preventing optical spillover, this design will also minimize the potential exchange of light-induced

metabolites between adjacent AALs, which could contribute in some degree to the nonindependence between measurements, especially during long light exposures, as for the study of dynamic light responses (see below). Although this source of measurement dependence cannot be completely excluded for optically continuous samples, its actual interference in the resulting LC can be minimized by decreasing the difference in light levels between AALs next to each other.

(4) AAL size. Large AALs should be used because more pixels will be considered for the estimation of fluorescence parameters, therefore reducing measuring errors. This can be of value in the case of samples showing a high physiological heterogeneity. Large AALs are also preferable because the actual area used for the calculation of fluorescence parameters (AOI) must be smaller than the maximum diameter of the AAL, to avoid border effects. The light mask used in this study had AALs of the same size and shape, disposed in linear arrays. However, masks may have AALs of different size or shape and arranged in any other way to better fit specific aspects of the sample or sample container. For instance, because under higher actinic irradiances a larger error is associated with the measurement of $\Delta F/F_m'$, AALs of higher light levels could be larger, resulting in more precise measurements due to the higher pixel number.

SPLCs

The method proposed here for the generation of LCs presents a number of innovations and significant advantages relative to conventional approaches. It enables one to (1) obtain nonsequential, temporally independent fluorescence measurements; (2) apply a large and variable number of actinic light levels with adequate replication; (3) generate a whole LC within the time required for a single measurement; and (4) define and control with unprecedented flexibility and ease of use the actinic light levels to be applied.

The considerable reduction of the total time required for the generation of a LC is one of the major advantages of this approach. As all light levels and replicates are measured simultaneously, the total duration of the LC will be essentially determined by the time defined for each individual measurement (e.g. for reaching a steady state), independent of the number of light levels and replicates. For example, for the case shown in Figure 5, the whole LC, consisting of 30 measurements (10 light levels $\times$ 3 replicates), could be finished after 6 min of light exposure, while it would have required a minimum of 3 h if each light level/sample was measured separately. This possibility is particularly useful when studying samples showing fast changes in their physiological state, as a response to stressors or changing environmental conditions, or associated with circadian rhythms (Rascher et al., 2001).

It is generally desirable for LCs to describe steady-state conditions. "Steady-state light curves" are largely independent from transient responses due to recent light history, making it easier to characterize the inherent physiological light response of a sample and to compare different samples. For the samples tested in this study, periods of 4 to 6 min of light mask exposure were enough to ensure a good characterization of the light response, allowing the estimation of LC parameters and the detection of differences in photoacclimation state. However, the time necessary to reach steady-state conditions depends greatly on the sample physiological state and previous light history. Also, because it is not likely that a steady state is reached at the same time for all actinic light levels, it is not possible to define a unique protocol for the application of the SPLC. Its application to samples of unknown physiological response should be preceded by preliminary monitoring of the variation over time of the fluorescence response under the different actinic light levels.

Dynamic Light Response

The proposed method also enables one to incorporate time in the study of the light response. The variation over time of fluorescence indices such as $\Delta F/F_m'$, rETR, or NPQ, like their light induction and dark relaxation kinetics, is of obvious interest for the characterization of the photophysiology of a sample. However, the patterns of variation during induction or relaxation strongly depend on the level of actinic light applied. In this context, the possibility of following the response to various actinic light levels simultaneously saves time, making it considerably easier to study the variation over time of the light response. This approach allows one to combine two types of studies that are often carried out separately: (1) LCs, in which actinic light intensity is varied while the time for measuring a response is arbitrarily fixed; and (2) induction/relaxation kinetics, in which actinic light intensity is arbitrarily fixed and the response is followed over time. It thus becomes possible to easily characterize the dynamic light response of a sample, describing both how the response to light varies with time and how the response kinetics varies with light.

An application of this possibility is the construction of LCs of fluorescence indices that require the comparison of measurements made at different times. This is the case of the coefficients that quantify the partitioning of nonphotochemical quenching in photoprotective (rapidly reversible) and photoinhibitory (slowly reversible) components. In most studies, these components are quantified for a single level of actinic light, usually arbitrarily defined to represent a stressful condition. By applying the proposed method, it became possible to easily generate LCs of the various quenching coefficients, a task that requires following the NPQ relaxation kinetics after exposure to various actinic light levels, which would otherwise be very time consuming.

Limitations

Despite the considerable advantages the method described here offers, there are a number of potential

limitations that must be considered. Although the results presented here are specific to the particular projector model used, these general limitations are likely applicable to any other models that share the same technology.

One limitation regards the range of actinic light levels possible to apply. On the one hand, it was not possible to obtain complete darkness, the minimum light intensity in the "dark" AALs being 5 μmol m^{-2} s^{-1}. This was due both to the limitations of the projector's output contrast and to the unavoidable light scattering originating from the illuminated areas. While this makes it impossible to measure parameters that require dark adaptation, like minimum (F_o) and maximum PSII fluorescence in the dark-adapted state (F_m), with the projector turned on, it does not affect significantly the construction of LCs, as 5 μmol m^{-2} s^{-1} can be considered sufficiently low for most applications. For the special case of NPQ versus E curves, which require the measurement of F_m (in the dark), the best alternative is to cover the projector's lens and determine F_m before the LC is started.

On the other hand, the maximum light intensity reached at the sample level may also represent a limitation for the construction of LCs. In the case of the setup used in this study, the maximum value of 1,125 μmol m^{-2} s^{-1} can be considered low when compared with the values reached by many commonly used PAM fluorometers, including imaging systems, generally reaching values above 2,000 μmol m^{-2} s^{-1}. Nevertheless, the actual limitation caused by the maximum light output will depend on the capacity to cover the relevant range of light intensities for each particular sample. For the plants used in this study, the range of actinic irradiances applied enabled us to characterize with adequate detail the light response of the various fluorescence parameters and indices, including the light-saturated part of the curve.

Another potential limitation derives from the relatively low sensitivity of imaging chlorophyll fluorometers. These imaging systems are based on CCD sensors, which are less sensitive than photodiodes or photomultipliers that equip the most common types of PAM fluorometers. This limits the detection of fluorescence signals, especially under high actinic light, when F_m' is lower and more difficult to discriminate from the F_s level. Accordingly, some manufacturers do not recommend measuring LCs with PAR levels above 700 μmol m^{-2} s^{-1} (Heinz Walz, 2009). This low sensitivity is expected to be overcome by using samples with a high chlorophyll *a* content but may limit the use of dilute microalgae or chloroplast suspensions.

Further Applications

This study aimed to show the main and most immediate applications of the method. Its use was illustrated on intact plant leaves, but it is potentially applicable to many other types of photosynthetic samples, ranging from large plant leaves, lichen, flat corals, macroalgae, or algal biofilms (microphytobenthos, periphyton) to phytoplankton or suspensions of microalgae, chloroplasts, or thylakoid suspensions, the main limitation being the chlorophyll *a* concentration. The use of optically separated samples, as on multiwell plates, is advantageous because it eliminates light spillover effects and ensures the independence of the measurements.

The results shown here were obtained using light masks with AALs that only differed regarding light intensity. However, the digital control of actinic light opens other possibilities. One is to manipulate the duration of light exposure so that, in the same experiment, replicated samples are exposed to different light doses given by different combinations of light intensity and exposure duration. Also, color may in principle be digitally manipulated and light masks can be made to incorporate AALs of different spectral composition. This would enable the possibility to compare the spectral responses of fluorescence indices.

A major result of this study is the introduction of digitally controlled illumination as a source of actinic light for photophysiological studies involving PAM fluorometry. It provides unprecedented flexibility in the control of the various aspects of a projected actinic light field. As this study showed, commercially available models of digital projectors, used in combination with commonly available software, may provide a readily accessible and inexpensive way of applying actinic light masks and generating SPLCs. However, such models were not built for this purpose, and their correct use requires some adaptations, namely regarding image flickering and changes in the light spectrum. We hope that this study may serve as a guideline for overcoming the limitations of currently available projectors and stimulate the development of dedicated equipment.

MATERIALS AND METHODS

Experimental Setup

The setup was composed of a combination of a PAM imaging chlorophyll fluorometer and a digital projector, used as an actinic light source (Fig. 1). The projector was positioned near the fluorometer's CCD camera in such a way that the projected light incided on the center of the area monitored by the fluorometer's camera (sampling area), optimizing the detection of the induced chlorophyll fluorescence. The projector was also positioned as vertically as possible (angle of 10° from vertical), to minimize asymmetries in the projected light field, and as close as possible to the sample (approximately 40 cm from the projector lens to the center of the sampling area), to maximize light intensity at the sample level.

Imaging Chlorophyll Fluorometer

The imaging chlorophyll fluorometer (Open FluorCAM 800-O/1010; Photon Systems Instruments) comprised four 13- × 13-cm light-emitting diode (LED) panels emitting red light (emission peak at 621 nm, 40-nm bandwidth) and a two-thirds inch CCD camera (CCD381) with an F1.2 (2.8–6 mm) objective. Two of the LED panels provided modulated measuring light (less than 0.1 μmol m^{-2} s^{-1}), and the other two provided saturating pulses (more than 7,500 μmol m^{-2} s^{-1}, 0.8 s). Chlorophyll fluorescence images (512 × 512 pixels, 695- to 780-nm spectral range) were captured and processed using FluorCam7 software (Photon Systems Instruments). When measuring long

sequences of fluorescence images (dynamic light response; see below), the FluorCam7 software was controlled by an AutoHotkey (version 1.1.09.00; available at www.autohotkey.com) script written to automatically run the protocol used for applying saturating pulses, save the fluorescence kinetics data for each measurement and export data as text files for further processing.

Digital Projector

All presented results were obtained using a LCD digital projector (EMP-1715; Epson) comprising a mercury arc lamp providing a light output of 2,700 lumens. A focusing lens was used to focus the projected images in the fluorometer's sampling area. The projected light field covered a rectangular area of approximately 14 × 10 cm. Projector settings were set to provide the widest range of light intensities at the sample level. With the above described setup configuration, PAR levels in the sampling area ranged between 5 and 1,125 μmol m^{-2} s^{-1}. Actinic PAR irradiance at the sample level was measured using a PAR microsensor (US-SQS/W; Heinz Walz) calibrated against a recently calibrated flat PAR quantum sensor (MQ-200; Apogee Instruments).

Actinic Light Mask

The digital projector was used to project an actinic light mask on the sampling area, consisting of a set of spatially separated AALs covering the range of PAR levels necessary to induce the fluorescence responses to be used to generate a light curve. The actinic light mask used in this study consisted of 30 circular AALs arranged in a 3 × 10 matrix, in which each array of 10 AALs corresponded to 10 different PAR values (5–1,125 μmol m^{-2} s^{-1}), arranged increasingly so that the highest values were closer to the projector (Fig. 1). Each AAL consisted of a circular homogenous light field of 4 mm in diameter. Adjacent AALs of the same array were separated by 1.0 mm. Three 10-AAL arrays were projected in parallel (1.5 mm apart), so that approximately the same light levels were applied on the three arrays. However, due to some unavoidable degree of heterogeneity in the projected light field, a small variation (on average less than 2.5%) was presented among replicated AALs.

The light mask was designed in Microsoft PowerPoint, using a code written in Microsoft Visual Basic to define the number, position, size, and shape (slightly oval to compensate for the inclination of the projector) of each AAL, as well as the light intensity and spectrum (through controlling the RGB code; see below). This code was used to automatically control the PAR level of each AAL, based on a relationship established between RGB settings and the PAR measured at the sample level.

The chlorophyll fluorescence emitted at each AAL was measured by defining AOI using FluorCam7 software. The AOIs were centered on the AALs but had a smaller diameter (approximately 3 mm) to minimize border effects that could otherwise introduce significant errors. On average, each AOI consisted of 32 pixels.

Actinic Light Spectrum

The spectrum of the light emitted by the digital projector was measured over a 350- to 1,000-nm bandwidth with a spectral resolution of 0.38 nm, using a USB2000 spectrometer (USB2000-VIS-NIR, grating #3; Ocean Optics; Serôdio et al., 2009). Light was collected using a 400-μm-diameter fiber optic (QP400-2-VIS/NIR-BX; OceanOptics) positioned perpendicularly to a reference white panel (WS-1-SL Spectralon Reference Standard; Ocean Optics) placed in the center of the sampling area of the fluorometer and the projected light field. A spectrum measured in the dark was subtracted from all measured spectra to account for the dark current noise of the spectrometer. Spectra were smoothed using a 10-point moving average filter.

LCs

LCs were generated by determining the fluorescence parameters F_s and F_m' for each AOI, each corresponding to a different irradiance level. F_s and F_m' were measured by averaging all pixel values of each AOI and averaging the fluorescence intensity during the 2 s immediately before the saturating pulse and during 0.6 s during the application of the saturating pulse (total duration of 800 ms), respectively. The kinetics of fluorescence intensity recorded immediately before and during the application of each saturating pulse was analyzed for each measurement using FluorCam7 software, and the parts of the fluorescence trace showing effects of the projector's light flickering were not considered for the estimation of F_s or F_m'. For each AOI (each E value), the rETR was calculated from the product of E and $\Delta F/F_m'$ (Genty et al., 1990):

$$\mathrm{rETR} = E \ \frac{F_m' - F_s}{F_m'} = E\ \Delta F/F_m' \quad (1)$$

Fluorescence measurements were also used to calculate the NPQ index, used to quantify the operation of photoprotective and photoinhibitory processes. NPQ was calculated from the relative difference between F_m and F_m':

$$\mathrm{NPQ} = \frac{F_m - F_m'}{F_m'} \quad (2)$$

For each AOI, F_m was measured at the end of a 20-min dark adaptation prior to light exposure. LCs were generated by applying a single saturating pulse after a defined period of light exposure (e.g. 6 min) following a 20-min dark adaptation period.

Dynamic Light Response

The potentialities of the method were further tested by characterizing the dynamic light response (i.e. the variation of the fluorescence light response over time). After a 20-min dark adaptation, samples were exposed to the light mask and saturating pulses were applied every 2 min. This rationale was also applied to light stress-recovery experiments, during which samples were subsequently exposed to darkness, to allow the characterization of the recovery after exposure to the various actinic light intensities. Data were used to calculate LCs and light kinetics (light induction and dark relaxation) of NPQ as well as the quenching coefficients partitioning NPQ into constitutive, photoprotective, and photoinhibitory components, according to Guadagno et al. (2010).

LC Models

rETR versus E curves were quantitatively described by fitting the model of Eilers and Peeters (1988) and by estimating the parameters α (the initial slope of the curve), maximum rETR ($\mathrm{rETR_m}$), and E_k:

$$\mathrm{rETR}(E) = \frac{E}{aE^2 + bE + c} \quad (3)$$

where

$$\alpha = \frac{1}{c},\ \mathrm{rETR_m} = \frac{1}{b + \sqrt{ac}} \text{ and } E_k = \frac{c}{b + \sqrt{ac}} \quad (4)$$

LCs of NPQ were described by fitting the model of Serôdio and Lavaud (2011) and by estimating the parameters maximum NPQ ($\mathrm{NPQ_m}$), irradiance corresponding to one-half of $\mathrm{NPQ_m}$ (E_{50}), and the sigmoidicity parameter (n):

$$\mathrm{NPQ}(E) = \mathrm{NPQ}_m \frac{E^n}{E_{50}^n + E^n} \quad (5)$$

The models were fitted using a procedure written in Microsoft Visual Basic and based on Microsoft Excel Solver. Model parameters were estimated iteratively by minimizing a least-squares function, forward differencing, and the default quasi-Newton search method (Serôdio and Lavaud, 2011).

Plant Material

The applicability of the method was illustrated on intact plant leaves. To compare the method in samples having distinct light responses, plants acclimated to contrasting light conditions were used. For HL-acclimated plants, leaves of common ivy (*Hedera helix*) grown under natural conditions were used. Photoperiod and weather conditions were those of November and December 2012 in Aveiro, Portugal: 10/14-h photoperiod, temperature range of 4°C to 16°C, relative humidity of 60% to 80%, precipitation of 100 to 200 mm, 95 to 120 insolation hours. For LL-acclimated plants, leaves of weeping fig (*Ficus benjamina*) grown in a greenhouse during the same time of year were used (average PAR of 20 μmol m^{-2} s^{-1}). All plants were grown in standard horticultural soil and watered every 2 d. These two species were selected also to illustrate the variability among leaf optical properties potentially affecting the measuring of fluorescence in closely located illuminated areas (light scattering within the leaf). Unless stated otherwise, all fluorescence measurements were made on the upper (adaxial) surface of the leaves.

ACKNOWLEDGMENTS

We thank Gonçalo Simões for invaluable technical help on the testing of digital projectors. This work benefited from discussions with Sónia Cruz, Jorge Marques da Silva, Paulo Cartaxana, and David Suggett.

Received September 19, 2013; accepted September 25, 2013; published September 25, 2013.

LITERATURE CITED

Eilers PHC, Peeters JCH (1988) A model for the relationship between light intensity and the rate of photosynthesis in phytoplankton. Ecol Modell **42:** 199–215

Genty B, Briantais JM, Baker NR (1989) The relationship between the quantum yield of photosynthetic electron transport and quenching of chlorophyll fluorescence. Biochim Biophys Acta **990:** 87–92

Genty B, Harbinson J, Baker NR (1990) Relative quantum efficiencies of the two photosystems of leaves in photorespiratory and non-photorespiratory conditions. Plant Physiol Biochem **28:** 1–10

Guadagno CR, Virzo De Santo A, D'Ambrosio N (2010) A revised energy partitioning approach to assess the yields of non-photochemical quenching components. Biochim Biophys Acta **1797:** 525–530

Heinz Walz (2009) PAM Imaging, M-series chlorophyll fluorometer, instrument description and information for users. Heinz Walz, Effeltrich, Germany

Henley WJ (1993) Measurement and interpretation of photosynthetic light-response curves in algae in the context of photoinhibition and diel changes. J Phycol **29:** 729–739

Herlory O, Richard P, Blanchard GF (2007) Methodology of light response curves: application of chlorophyll fluorescence to microphytobenthic biofilms. Mar Biol **153:** 91–101

Ihnken S, Eggert A, Beardall J (2010) Exposure times in rapid light curves affect photosynthetic parameters in algae. Aquat Bot **93:** 185–194

Johnson ZI, Sheldon TL (2007) A high-throughput method to measure photosynthesis-irradiance curves of phytoplankton. Limnol Oceanogr Methods **5:** 417–424

Lavaud J, Strzepek RF, Kroth PG (2007) Photoprotection capacity differs among diatoms: possible consequences on the spatial distribution of diatoms related to fluctuations in the underwater light climate. Limnol Oceanogr **52:** 1188–1194

Lefebvre S, Mouget J-L, Lavaud J (2011) Duration of rapid light curves for determining the photosynthetic activity of microphytobenthos biofilm *in situ*. Aquat Bot **95:** 1–8

Müller P, Li XP, Niyogi KK (2001) Non-photochemical quenching: a response to excess light energy. Plant Physiol **125:** 1558–1566

Perkins RG, Mouget JL, Lefebvre S, Lavaud J (2006) Light response curve methodology and possible implications in the application of chlorophyll fluorescence to benthic diatoms. Mar Biol **149:** 703–712

Ralph PJ, Gademann R (2005) Rapid light curves: a powerful tool to assess photosynthetic activity. Aquat Bot **82:** 222–237

Rascher U, Hütt MT, Siebke K, Osmond B, Beck F, Lüttge U (2001) Spatiotemporal variation of metabolism in a plant circadian rhythm: the biological clock as an assembly of coupled individual oscillators. Proc Natl Acad Sci USA **98:** 11801–11805

Rascher U, Liebig M, Lüttge U (2000) Evaluation of instant light-response curves of chlorophyll fluorescence parameters obtained with a portable chlorophyll fluorometer on site in the field. Plant Cell Environ **23:** 1397–1405

Rohácek K (2010) Method for resolution and quantification of components of the non-photochemical quenching (q_N). Photosynth Res **105:** 101–113

Schreiber U, Bilger W, Neubauer C (1994) Chlorophyll fluorescence as a nonintrusive indicator for rapid assessment of in vivo photosynthesis. *In* **Shulze ED, Caldwell MM**, eds, Ecophysiology of Photosynthesis. Springer-Verlag, Berlin, pp 49–70

Schreiber U, Gademann R, Ralph PJ, Larkum AWD (1997) Assessment of photosynthetic performance of *Prochloron* in *Lissoclinum patella* in hospite by chlorophyll fluorescence measurements. Plant Cell Physiol **38:** 945–951

Schreiber U, Klughammer C, Kolbowski J (2012) Assessment of wavelength-dependent parameters of photosynthetic electron transport with a new type of multi-color PAM chlorophyll fluorometer. Photosynth Res **113:** 127–144

Schreiber U, Schliwa U, Bilger W (1986) Continuous recording of photochemical and nonphotochemical chlorophyll fluorescence quenching with a new type of modulation fluorometer. Photosynth Res **10:** 51–62

Seaton GGR, Walker DA (1990) Chlorophyll fluorescence as a measure of photosynthetic carbon assimilation. Proc Biol Sci **242:** 29–35

Serôdio J, Cartaxana P, Coelho H, Vieira S (2009) Effects of chlorophyll fluorescence on the estimation of microphytobenthos biomass using spectral reflectance indices. Remote Sens Environ **113:** 1760–1768

Serôdio J, Ezequiel J, Barnett A, Mouget J, Méléder V, Laviale M, Lavaud J (2012) Efficiency of photoprotection in microphytobenthos: role of vertical migration and the xanthophyll cycle against photoinhibition. Aquat Microb Ecol **67:** 161–175

Serôdio J, Lavaud J (2011) A model for describing the light response of the nonphotochemical quenching of chlorophyll fluorescence. Photosynth Res **108:** 61–76

Serôdio J, Vieira S, Cruz S, Barroso F (2005) Short-term variability in the photosynthetic activity of microphytobenthos as detected by measuring rapid light curves using variable fluorescence. Mar Biol **146:** 903–914

Serôdio J, Vieira S, Cruz S, Coelho H (2006) Rapid light-response curves of chlorophyll fluorescence in microalgae: relationship to steady-state light curves and non-photochemical quenching in benthic diatom-dominated assemblages. Photosynth Res **90:** 29–43

Smith EL (1936) Photosynthesis in relation to light and carbon dioxide. Proc Natl Acad Sci USA **22:** 504–511

Walters RG, Horton P (1991) Resolution of components of non-photochemical chlorophyll fluorescence quenching in barley leaves. Photosynth Res **27:** 121–133

White AJ, Critchley C (1999) Rapid light curves: a new fluorescence method to assess the state of the photosynthetic apparatus. Photosynth Res **59:** 63–72

Ye ZP, Robakowski P, Suggett DJ (2013) A mechanistic model for the light response of photosynthetic electron transport rate based on light harvesting properties of photosynthetic pigment molecules. Planta **237:** 837–847